PCCP

PAPER

View Article Online
View Journal | View Issue

CrossMark click for updates

Cite this: *Phys. Chem. Chem. Phys.*, 2016, **18**, 19173

Low-field thermal mixing in [1-^{13}C] pyruvic acid for brute-force hyperpolarization

David T. Peat,[a] Matthew L. Hirsch,[b] David G. Gadian,[a] Anthony J. Horsewill,[a] John R. Owers-Bradley*[a] and James G. Kempf*[b]

Received 28th April 2016,
Accepted 23rd June 2016

DOI: 10.1039/c6cp02853e

www.rsc.org/pccp

We detail the process of low-field thermal mixing (LFTM) between ^{1}H and ^{13}C nuclei in neat [1-^{13}C] pyruvic acid at cryogenic temperatures (4–15 K). Using fast-field-cycling NMR, ^{1}H nuclei in the molecule were polarized at modest high field (2 T) and then equilibrated with ^{13}C nuclei by fast cycling (~300–400 ms) to a low field (0–300 G) that activates thermal mixing. The ^{13}C NMR spectrum was recorded after fast cycling back to 2 T. The ^{13}C signal derives from ^{1}H polarization *via* LFTM, in which the polarized ('cold') proton bath contacts the unpolarised ('hot') ^{13}C bath at a field so low that Zeeman and dipolar interactions are similar-sized and fluctuations in the latter drive ^{1}H–^{13}C equilibration. By varying mixing time (t_{mix}) and field (B_{mix}), we determined field-dependent rates of polarization transfer ($1/\tau$) and decay ($1/T_{1m}$) during mixing. This defines conditions for effective mixing, as utilized in 'brute-force' hyperpolarization of low-γ nuclei like ^{13}C using Boltzmann polarization from nearby protons. For neat pyruvic acid, near-optimum mixing occurs for t_{mix} ~ 100–300 ms and B_{mix} ~ 30–60 G. Three forms of frozen neat pyruvic acid were tested: two glassy samples, (one well-deoxygenated, the other O_2-exposed) and one sample pre-treated by annealing (also well-deoxygenated). Both annealing and the presence of O_2 are known to dramatically alter high-field longitudinal relaxation (T_1) of ^{1}H and ^{13}C (up to 10^2–10^3-fold effects). Here, we found smaller, but still critical factors of ~(2–5)× on both τ and T_{1m}. Annealed, well-deoxygenated samples exhibit the longest time constants, *e.g.*, τ ~ 30–70 ms and T_{1m} ~ 1–20 s, each growing *vs.* B_{mix}. Mixing 'turns off' for B_{mix} > ~100 G. That $T_{1m} \gg \tau$ is consistent with earlier success with polarization transfer from ^{1}H to ^{13}C by LFTM.

Open Access Article. Published on 24 June 2016. Downloaded on 8/12/2024 11:40:28 PM.
This article is licensed under a Creative Commons Attribution 3.0 Unported Licence.

Introduction

Low-field thermal mixing (LFTM) is the process by which dissimilar spins in a solid sample are brought to mutual equilibrium by exposure to a magnetic field small enough that their magnetic resonance lineshapes come into overlap.[1–3] In this way, mutual spin flips can occur with conservation of energy, allowing the noted equilibration, *e.g.*, among heteronuclei in NMR (nuclear magnetic resonance). This phenomenon is of special recent interest as a way to hyperpolarize low-γ nuclear spins (γ = gyromagnetic ratio) such as ^{13}C, ^{15}N or ^{31}P, using spin order originally established in high-γ nuclei like ^{1}H.[4,5] From a thermodynamic viewpoint, LFTM is a process of rapid cooling, in which a highly polarized (cold) bath of spins is made to strongly couple with poorly polarized (hot) spins. For mixing ^{1}H with low-γ nuclei, the protons have much larger specific heat (proportional to γ^2), and thus dominate in establishing the final 'spin temperature'.[1–3] The result is a cold (highly polarized) set of low-γ spins.

Hyperpolarization is a potentially transformative approach to dramatically enhance sensitivity in solution NMR and magnetic resonance imaging (MRI). Orders-of-magnitude gains are available from solids-into-liquids methods like the 'brute-force' approach[4–7] (yielding 10^2 to 10^4-fold enhancements) and dissolution dynamic nuclear polarization[8] (d-DNP, for >10^4-fold). Methods to hyperpolarize directly in the liquid state are also promising, especially using parahydrogen (p-H_2).[9,10] This can yield >10^4-fold polarization gains in molecules reacting with p-H_2,[11] but has limits due to chemical specificity in transferring p-H_2 spin order into a molecule of interest. Direct DNP in liquids is also well known, but typically limited to non-polar solvents and lower fields,[12,13] while optically pumped methods also warrant interest,[14] as are approaches in which molecular carriers of hyperpolarized xenon can enable *in vivo* imaging applications.[15–19]

Among generally applicable methods of hyperpolarization, the brute-force approach is a natural fit with LFTM. In brute force, a large Boltzmann polarization is built up on protons at high field and low temperature (*e.g.*, B = 14 T, T = 100 mK to 2 K). Protons are the preferred starting point, offering polarization build-up that can be >10-fold faster than for low-γ nuclei. And yet the ultimate goal is usually hyperpolarization of a low-γ

[a] *School of Physics & Astronomy, University of Nottingham, Nottingham NG7 2RD, UK. E-mail: John.Owers-Bradley@nottingham.ac.uk*
[b] *Bruker Biospin Corp., 15 Fortune Drive, Billerica, MA 01821, USA. E-mail: James.Kempf@bruker.com*

Open Access Article. Published on 24 June 2016. Downloaded on 8/12/2024 11:40:28 PM.
This article is licensed under a Creative Commons Attribution 3.0 Unported Licence.

species like ^{13}C for use as an ultrasensitive, background-free agent for MRI.[20–22] LFTM is a way to get the best of both worlds without resorting to an NMR pulse sequence, which could likewise effect a polarization transfer but at the expense of limiting the amount of sample by confinement to a radiofrequency (RF) coil.

In recent experiments,[5,7] brute-force was married with LFTM in application to ^{13}C-labeled pyruvic acid. Protons equilibrated to noted high-B, low-T conditions were used to hyperpolarize ^{13}C when the sample was ejected from the polarizer and through a low field region (<100 G). After either immediate aqueous dissolution,[5] or off-site transport followed by dissolution,[7] hyperpolarized ^{13}C was observed by solution NMR. Enhancements of 100–1000× were obtained in pyruvic acid and other molecules. That corresponded to up to 0.2% ^{13}C polarization, with potential to reach >10%, which is more than 10^4 times more than thermal equilibrium levels (~0.0001% to 0.001%) for ^{13}C in MRI and solution NMR.

Pyruvic acid is the hottest current target for medical imaging with hyperpolarization.[23] It and other small-molecule metabolites have rates of cellular uptake and chemical conversion that vary with tissue health.[20–22] Tracking such processes by MRI already enables detection and grading of various cancers[23–28] or cardiac function.[29–31] These approaches depend absolutely on hyperpolarization. Though labelling with a low-γ nucleus provides the huge advantages of chemically specific, background-free detection, as well as much longer polarization lifetimes, it also requires hyperpolarization to overcome the γ^2-to-γ^3 dependence of sensitivity, on top of the disadvantage of low metabolite concentration.

Here, we define conditions necessary for effective LFTM in [1-^{13}C] pyruvic acid and compare to those used in recent brute-force experiments. We start by detailing various physical conditions of frozen, neat pyruvic acid relevant to brute force. That includes samples that are or are not well-deoxygenated, and those rapidly frozen or subsequently annealed. Temperature-dependent ^{1}H longitudinal relaxation times (T_1) are presented to highlight differences among these samples. We then extend that knowledge by exploring effects of O_2-exposure and annealing on LFTM. That includes quantifying build-up and decay with LFTM *vs.* the size of the mixing field and the duration of exposure. Time constants for ^{1}H–^{13}C equilibration and eventual decay are quantified *via* the build-up and loss of ^{13}C signal intensity *vs.* duration of the mixing period. Finally, in addition to investigating optimum conditions for LFTM, we also determine the threshold field above which mixing becomes inactive due to removal of ^{1}H–^{13}C spectral overlap.

Results

The pyruvic acid samples studied here were all neat, frozen solids (no additives or co-solvents) as utilized in recent brute-force experiments[5] to hyperpolarize ^{13}C and in further work to transport[7] the hyperpolarization from the polarizer to a remote imaging centre. Here, in addition to detailing LFTM of ^{1}H and ^{13}C in such samples, we also explore the importance of certain sample-handling protocols. In particular, both annealing[32] and deoxygenation of samples are known to induce large changes in longitudinal relaxation times (T_1) of ^{1}H and ^{13}C. In this study, we explore LFTM in [1-^{13}C] pyruvic acid, and also changes in the mixing that occur in cases of partial sample annealing and exposure to oxygen.

The relevant temperature range of the current study is >4 K. Although brute force relies on polarization in conditions of low (<2 K) or ultralow (<500 mK) temperature, higher cryogenic temperatures are critical in post-polarization steps of sample extraction, thermal mixing, transport and dissolution. For example,

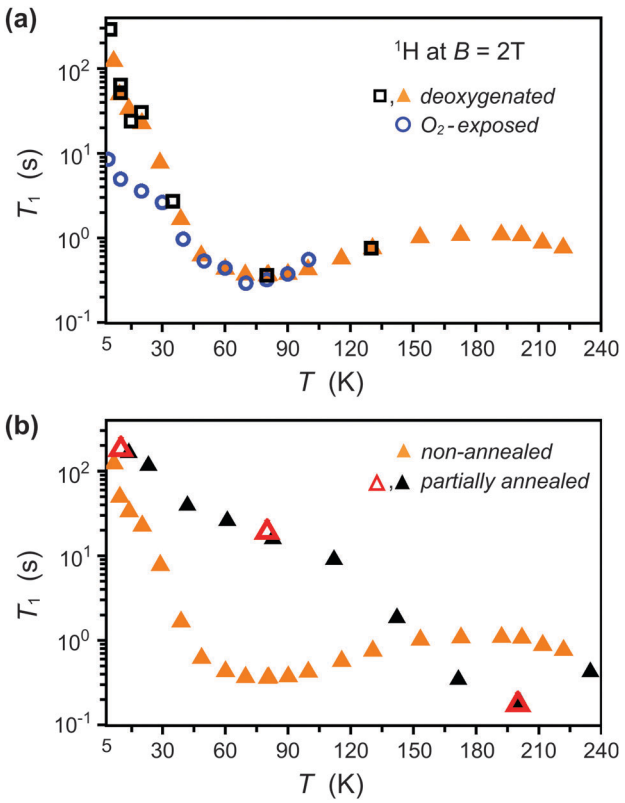

Fig. 1 Profiles of T_1(^{1}H) *vs.* temperature for [1-^{13}C] pyruvic acid. (a) From non-annealed samples. The full profile from a deoxygenated sample (▲) is as previously described,[7] and was collected in a flame-sealed quartz tube and distinct NMR apparatus. Here, in the fast-field-cycling (FFC) apparatus, we collected T_1 profiles from two non-annealed samples: one O_2-exposed (○), the other (□) deoxygenated and well-sealed. (See Materials and Methods for alternative sealing approach needed for samples tested in the FFC apparatus.) O_2 exposure gave up to >10× faster relaxation at low temperatures (4–30 K). The present deoxygenated sample (□) exhibits a T_1 profile matching earlier results (▲), thus demonstrating on-par exclusion of O_2 for a sample to be studied by FFC. (b) T_1 profile following partial/intermediate annealing (△) of the well-deoxygenated sample [*i.e.*, of same sample as □ in (a)]. This annealing yielded tremendous change in the T_1 profile, matching earlier results (▲) obtained in noted separate apparatus.[7] The intermediate annealing protocol is described in Materials and Methods. It yielded nearly 10^2-fold slower relaxation at the centre of the 'T_1 valley' *vs.* a non-annealed sample [▲, same data as in (a)]. All data in (a and b) were collected at 2.0 or 2.1 T, excepting one set (▲) in (b) from 4.2 T. The latter is intended as overview of the overall pattern of intermediate-annealed behaviour. The distinct field has insignificant impact (~2×) on T_1 compared to ~100× changes induced by this degree of annealing.

This journal is © the Owner Societies 2016

Open Access Article. Published on 24 June 2016. Downloaded on 8/12/2024 11:40:28 PM.
This article is licensed under a Creative Commons Attribution 3.0 Unported Licence.

during the lead-up to extraction from a brute-force polarizer, sample warming occurs (5–15 K for 30–60 s), and further changes may occur in the step of ejection in concert with LFTM. Finally, 4–80 K is relevant for transport.

As background to the thermal-mixing story, Fig. 1 displays temperature-dependent impacts of both oxygenation and annealing on the high-field T_1 of protons in pyruvic acid. Fig. 1(a) focuses on oxygenation. Because O_2 is paramagnetic, it can induce nuclear spin relaxation *via* motions relative to the surrounding bath of frozen pyruvic acid. T_1 *vs.* temperature is shown for two well-deoxygenated, well-sealed samples and one that had been exposed to air. For each, a characteristic 'valley' profile is apparent with minimum near 75 K, the temperature at which methyl rotations have the greatest spectral density near relevant NMR frequencies. Below ~45 K, sharply rising T_1 values result in >100-fold slower relaxation near 5–10 K in well-deoxygenated cases. If instead, O_2 is present, the steep rise is significantly attenuated, as seen in data from a sample that, although originally deoxygenated, was exposed to air before its introduction to the helium-atmosphere cryostat of the fast field-cycling (FFC) apparatus. That resulted in ~30-fold faster T_1 relaxation near 4.2 K compared to the well-sealed sample. [See Fig. 1 caption and Materials and Methods for details on deoxygenation, sample sealing and the mild exposure to O_2/air that yielded such changes.]

Next, we explored annealing directly in the FFC apparatus. Prolonged exposure to temperature above a glass transition (T_g) enables structural organization at the atomic and molecular scale. Resulting morphology can be fixed by subsequent cooling and maintenance of the sample below T_g. In brute-force hyperpolarization, such annealing can be critical in order to obtain spin-relaxation properties that are favourable during periods used to prepare for and execute sample extraction and/or transport of a hyperpolarized sample.[7] For neat pyruvic acid, T_g of ~215–230 K was previously discovered.[32]

Fig. 1(b) shows dramatic changes in the T_1 profile for frozen pyruvic acid after thermal conversion to a form intermediate between non- and fully annealed states.[7,32] For example, intermediate annealing here increases T_1 by >100× at 75 K, which is the valley centre for the non-annealed form. The conditioning that led to this change (see Materials and Methods) is akin to that used in recent brute-force experiments,† where corresponding changes in T_1 were critical to success.[5,7] In particular, intermediate annealing removes the T_1 valley that otherwise would range across 4 to 150 K in non-annealed pyruvic acid. The changed shape of the ^{1}H profile [Fig. 1(b)] occurs very similarly at the 1-^{13}C site.[32]

This apparent removal of the valley mitigates post-polarization losses during preparation for ejection as well as thermal mixing, storage, transport and ultimate dissolution. The physical origins of the changes in T_1 relate to structural rearrangement during annealing (or partial annealing). A consistent picture is that a new morphology results that restricts methyl rotation. As a consequence, higher temperature is required to match the spectral density of rotations with NMR transitions. Correspondingly, Fig. 1(b) shows the T_1 valley minimum shifted up to ~200 K *vs.* ~75 K for non-annealed pyruvic acid. More-complete annealing[7,32] (not shown) similarly positions the T_1 minimum near 200 K, but also yields a steeper rise when the temperature drops below ~125 K. With that, a fully annealed sample maintains the 10^2-fold T_1 gap relative to non-annealed all the way down to 4–10 K. Thus far, only intermediate-annealed samples of pyruvic acid have been tested with brute-force hyperpolarization, and the current study of LFTM is similarly focused on this degree of annealing.

To define the low-field range appropriate for thermal mixing, as well as associated time constants for equilibration and loss

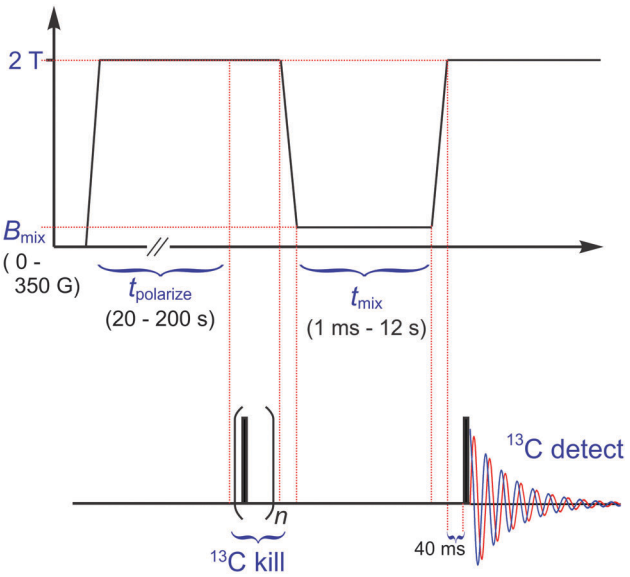

Fig. 2 Pulse sequence for characterization of low-field thermal mixing. The opening period (~1 s) at zero field erases the spin magnetization of all nuclei. The subsequent period (20–200 s) at 2.0 T polarizes ^{1}H sufficiently for good signal-to-noise in ^{13}C after equilibration of the two nuclei. To ensure zero input polarization from ^{13}C for the mixing period, a preceding ^{13}C kill sequence (n = 40 π/2 pulses at 350 μs intervals) was incorporated.‡ Subsequent fast field cycling (~330 ms at 6 T s^{-1}) brings the sample to the field of choice (*e.g.*, B_{mix} = 0–350 G) for thermal mixing at duration t_{mix} = 0.001–12 s. At the shortest of these time points, the exact field value may be skewed somewhat due to a settling time expected to be up to 40 ms. The return to 2.0 T (~400 ms at 5 T s^{-1}) after mixing incorporates a 40 ms settling period to ensure stable, resonant ^{13}C detection after the single π/2 pulse indicated.

† Distinct dimensions and geometry of the sample may impact annealing. Samples here were ~4 mm OD by 10 mm long solid cylinders. Earlier brute-force experiments used samples of similar diameter and length, but frozen as a hollow, thin (~1 mm) cylinder. It has not been discounted that such geometry might change response to annealing. T_1 *vs.* temperature has not been measured for the hollow cylinder case.

‡ The ^{13}C kill sequence might be thought unnecessary because an effective mixing period will peg ^{13}C polarization only according to the pre-mixing polarization level on ^{1}H, almost regardless of starting ^{13}C polarization.[5] The reason is that the 'spin specific heat' [ref. 1, 2 and 5] of protons is 100-fold larger than for ^{13}C in pyruvic acid (and most all protonated molecules, even at 99% ^{13}C). Nonetheless, a signal of dominant origins in ^{1}H polarization is only guaranteed when mixing is active, *i.e.*, for just a portion of the full (t_{mix}, B_{mix}) space we tested. Thus, the ^{13}C kill is needed when t_{mix} is not on the timescale of equilibration and/or when B_{mix} is above the mixing threshold.

Open Access Article. Published on 24 June 2016. Downloaded on 8/12/2024 11:40:28 PM.
This article is licensed under a Creative Commons Attribution 3.0 Unported Licence.

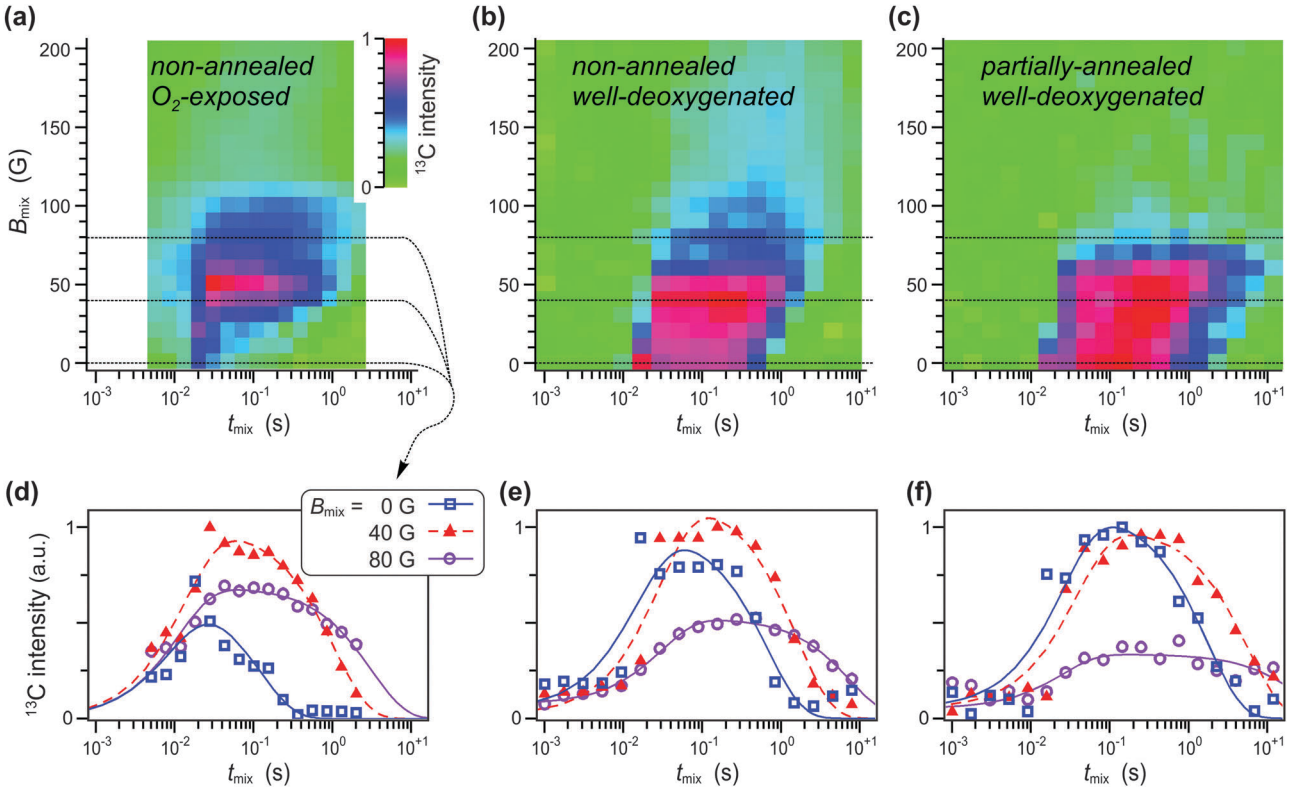

Fig. 3 ^{13}C-detected low-field thermal mixing signal intensity derived from ^{1}H polarization in [1-^{13}C] pyruvic acid. Upper (2D) and lower (1D) plots are pairs corresponding to samples that were (a and d) O_2-exposed, non-annealed, (b and e) well-deoxygenated, non-annealed, and (c and f) well-deoxygenated, intermediate-annealed. Each sample corresponds to a T_1 profile in Fig. 1, as noted in the main text. In 2D plots of (a–c), a shading scale maps the t_{mix} and B_{mix} dependencies of ^{13}C signal intensity gained by low-field contact with the proton bath. [The shading scale shown in (a) also applies to (b and c), although each data set was normalized individually and no quantitative intensity comparison among sample types is implied, as recycle delays shorter than the sample-dependent values of $T_1(^1H)$ were used. The normalized scale is, however, identical for each upper/lower pair of plots.]. Corresponding fixed-field slices in (d–f) are plotted for B_{mix} = 0 G (—□—), 40 G (– ▲ –) and 80 G (—○—), where each curve is a fit to eqn (1). All data sets were obtained using the NMR pulse sequence of Fig. 2. Data in (a and d) and (b and e) were collected at 4.2 K, whereas the rightmost set [(c and f), intermediate annealed] was collected at 10 K. That these sets are comparable, in spite of the temperature difference, was demonstrated by repetition of (b) at 10 K. In spite of poorer signal-to-noise, this did show the same intensity pattern as here, as well as nearly indistinguishable results from fits to eqn (1) (see ahead, Fig. 5). Furthermore, one slice (at 50 G) was repeated for the partially annealed sample (c) at 4.2 K and yielded rise and fall times indistinguishable from those at 10 K (see Materials and Methods).

of polarization in the ^{1}H–^{13}C system, we used the NMR sequence of Fig. 2. The time sequence of FFC events is shown, as synchronized with an RF pulse sequence. Although pulses are only applied to ^{13}C, both ^{1}H and ^{13}C have clearly defined roles in the experiment. The FFC sequence moves the spin system through events

(i) to ensure all ^{1}H and ^{13}C spin order is destroyed *via* an initial period at zero field,

(ii) to polarize ^{1}H nuclei at high field (*e.g.*, 2 T),

(iii) to mix ^{1}H polarization with ^{13}C *via* exposure to low-field (B_{mix} = 0–350 G) for time t_{mix} = 0.001–12 s,

and, finally,

(iv) to detect resulting ^{13}C magnetization *via* NMR after returning to high field.

For present experiments at or below 20 K, the field cycling is fast (<400 ms) compared to the timescale of high-field (*e.g.*, >500 G = 0.05 T) longitudinal relaxation. Faster processes turn on at some point below 500 G (*e.g.*, thermal mixing). However, the cycling rate requires only ~10 ms to cover 500 G plus similar time for settling. (See caption to Fig. 2 and Materials and Methods for details.) Observations ahead indicate that this is fast enough for at least semi-quantitative determination of all time constants operative during the LFTM experiment.§

Results of mixing studies are shown in Fig. 3. 2D plots of ^{13}C signal intensity *vs.* B_{mix} and t_{mix} are shown in (a–c) for three of the same frozen [1-^{13}C] pyruvic acid samples used in the above T_1 study. Namely, Fig. 3(a) is from the O_2-exposed, non-annealed sample [○ from Fig. 1(a)], Fig. 3(b) is from well-deoxygenated, non-annealed [□ from Fig. 1(a)], and Fig. 3(c) is also well-deoxygenated, but intermediate-annealed [△ from Fig. 1(b)]. All three samples reveal a thermal-mixing 'hot spot'

§ About 3–4 ms was required to drop from 200 G to zero field, where 200 G is conservatively high for the threshold above which mixing ceases for [1-^{13}C] pyruvic acid. This few ms ramping through LFTM-active fields might skew interpretation of the mixing rise time (τ), especially for data collected at the lowest values of B_{mix}.

This journal is © the Owner Societies 2016

Open Access Article. Published on 24 June 2016. Downloaded on 8/12/2024 11:40:28 PM.
This article is licensed under a Creative Commons Attribution 3.0 Unported Licence.

that results in greatest ^{13}C intensity centered near (B_{mix}, t_{mix}) ~ (50 G, 100 ms).

Qualitative comparison of Fig. 3(a) to the 2D plots in (b and c) reveals that O_2-exposure limits the degree of ^{13}C intensity that LFTM is able to establish for mixing, particularly below B_{mix} = 50 G. For more quantitative analysis, we fit individual time slices at constant B_{mix} to

$$I(t_{mix}) = I_0\left(1 - e^{-t_{mix}/\tau}\right)e^{-t_{mix}/T_{1m}}, \quad (1)$$

where I_0 is overall intensity, τ is the time constant for mutual equilibration of ^1H and ^{13}C and T_{1m} is the time constant for decay. Note that the decay process is distinct from longitudinal relaxation. In fact, T_{1m} describes mutual decay of order in a combined spin system (here of ^1H and ^{13}C) whose quantization is set not solely by the Zeeman interaction, but rather by similar-sized dipolar and Zeeman terms of the multinuclear Hamiltonian.

Individual fits to eqn (1) of slices from Fig. 3(a–c) are correspondingly shown in Fig. 3(d–f). Each data set and curve shows an initial rise in ^{13}C intensity (typically τ < 50 ms) followed by the much slower decay process (T_{1m} typically ranging 1–20 s). Initial rises in Fig. 3(d–f) often deviate from the fitted curve. This may be due to moderately skewed early response caused by ramping to and settling at B_{mix}. Thus, fitted τ values are likely less accurate than the T_{1m} values. Nonetheless, detailed accuracy is not essential to assess the general timescale needed for effective mixing, nor are we prevented from making reliable relative comparisons of trends between samples with varied oxygenation and/or annealing.

For closer analysis, Fig. 4 plots all fitted parameters for the three varieties of sample. Fig. 4(a) gives overall intensity *vs.* B_{mix}. (Each sample normalized for $I_{0,max}$ = 1.) This again emphasizes that O_2 exposure reduces the ^{13}C polarization achievable for B_{mix} < 50 G. In fact, LFTM efficacy is sharply peaked in that case, and so oxygenation, even by apparently mild exposure to air, can require especially precise conditions to achieve productive ^1H–^{13}C equilibration.

The situation is more forgiving for a well-deoxygenated sample. Fig. 4(a) shows that the intensity profiles for the two O_2-free cases tested here are relatively flat over B_{mix} = 0–50 G. Partial annealing yields particularly consistent intensity over this range. Meanwhile both non- and intermediate-annealed samples show similar falloff as B_{mix} increases from 50 to 100 G. Slight ^{13}C intensity lingers up to 200 G, especially in the non-annealed case, a fact that is especially apparent in the corresponding 2D profile of Fig. 3(b). However, signal-to-noise begins to limit fit quality for traces *vs.* t_{mix} at the largest B_{mix} values. Finally, we observed almost no ^{13}C intensity for traces collected at B_{mix} = 250, 300 and 350 G for each of the three samples (data not shown). That indicates that LFTM is no longer effective above a threshold of approximately 200 G for this sample.

The intensity variations are explained by sample-to-sample variation of τ and T_{1m}. First, in Fig. 4(b), the O_2-exposed sample shows significantly reduced equilibration times (τ ~ 5–15 ms), all less than the smallest value from each of the well-deoxygenated samples (τ ~ 20 ms at B_{mix} = 0). Furthermore, those two profiles

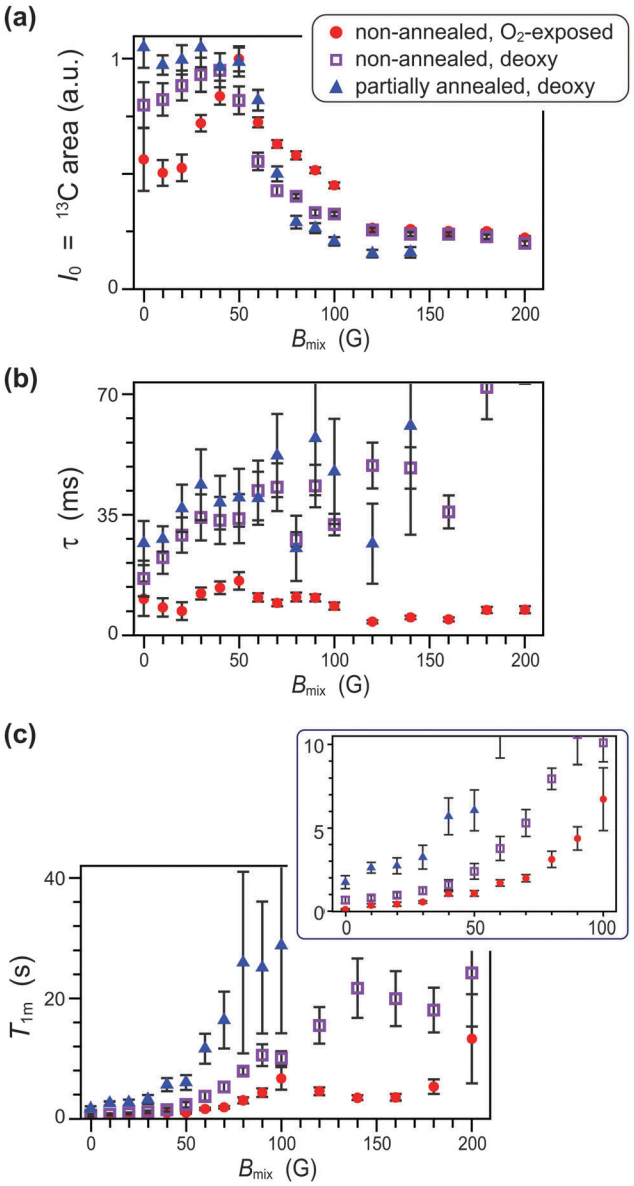

Fig. 4 Parameters of thermal mixing at 4.2 K. Showing (a) I_0, the ^{13}C intensity, (b) τ, the ^1H–^{13}C mixing time constant, and (c) T_{1m}, the common relaxation time constant for decay of order in the ^1H–^{13}C spin system. Each plot shows results for a non-annealed and O_2-exposed sample (closed circle, ●) along with those for non-annealed, de-oxygenated (open square, □) and intermediate-annealed de-oxygenated (closed triangle, ▲) samples. Fit parameters correspond to eqn (1). Uncertainties are the asymptotic standard error reported by *Mathematica*'s nonlinear regression routine. Large uncertainties for the highest T_1 values are due primarily to collection of data up to only t_{mix} = 12 s.

continue to rise from τ ~ 30 to >60 ms as B_{mix} increases over the LFTM-active range (*i.e.*, up to ~150–200 G). The faster equilibration observed when paramagnetic O_2 is present is likely due to electron-assisted LFTM. For example, few-spin processes may occur involving mutual flips of ^1H, ^{13}C and an electron(s), as resonances of the latter overlap with nuclear lines at these low fields. Also, electron-induced broadening may extend the range of B_{mix} over which ^1H–^{13}C overlap is sufficient for LFTM.

Open Access Article. Published on 24 June 2016. Downloaded on 8/12/2024 11:40:28 PM.
This article is licensed under a Creative Commons Attribution 3.0 Unported Licence.

Similar impact is apparent in the plots of decay time constants, T_{1m} *vs.* B_{mix} in Fig. 4(c). At all values of B_{mix}, the O_2-exposed sample exhibits fastest relaxation and partially annealed exhibits the slowest. Deoxygenation appears to be especially critical. For example, in a typical mixing event employed in recent brute-force studies (500 ms, near 50 G),[5,7] T_{1m} losses would be roughly 40% for O_2-exposed, 10% for deoxygenated and $<5\%$ for partially annealed (and deoxygenated) sample variants. Even worse can be expected at mixing fields <50 G, where the same transit time can yield $>90\%$ loss for an O_2-exposed sample. These facts echo our point above: although thermal mixing can work in the presence of O_2, great care would be needed to select and reproduce successful conditions. It is simply much better and more straightforward to carefully exclude O_2.

The results also quantify the value of annealing a sample to maintain ^{13}C polarization gained by LFTM. Fig. 4(b) already shows that the partial annealing has no drawback on the rate of ^{1}H–^{13}C equilibration. Only modest impact was observed, *i.e.*, an average of $\sim$20% longer τ relative to non-annealed. Because the added build-up time is on the tens-of-milliseconds scale and occurs within a hundreds-of-milliseconds event (*i.e.*, sample extraction in a brute-force experiment), there is no sacrifice. More important is the benefit from partial annealing, which approximately doubles T_{1m} over a range of B_{mix} values. For the most important mixing fields (0–100 G), T_{1m} runs from $\sim$2.6 s to 30 s for the partially annealed form, *vs.* only 0.8 s to 15 s for the non-annealed and deoxygenated sample. Annealing is thus a very effective protection against polarization loss in brute-force experiments. For example, extracting a sample from a high-field polarizing environment ($\sim$14 T) through a mixing field of <100 G is practical on the 1 s time scale, whereas dropping to the 100 ms timescale in order to achieve similar loss for a non-annealed sample would push the limits of practical sample ejection, or require modifications to keep B above the mixing threshold for a greater portion of the eject path.

A final point of interest on parameter variation *vs.* B_{mix} is that all three sample variations exhibit a rising T_{1m} for B_{mix} up to about 100 G. Subsequent drop-offs occur near 100–150 G, depending on the sample. For now, this is unexplained, but reproducible. Four other 2D profiles collected from O_2-exposed samples had the same roughly parabolic increase of T_{1m} up to $B_{mix} \sim 100$ G, followed by a dip between 100–200 G. Similar behavior is apparent in the other two sample variations tested, but with a T_{1m} 'peak' at slightly higher B_{mix}. The abrupt apparent change might be caused by entry into a new regime near or above the LFTM threshold, where eqn (1) no longer applies. That transition may reflect a switching off of LFTM or new importance of 3-spin mixing events involving ^{1}H and two ^{13}C nuclei. The latter process has been used to explain mixing of ^{7}Li and ^{19}F in LiF crystals at 75 G.[1–3] It might also be that 3-spin mixing explains the long tail of ^{13}C intensity *vs.* B_{mix}, *e.g.*, where I_0 does not quite go to zero at 200 G in Fig. 4(a).

Finally, thermal-mixing behavior at somewhat higher temperatures is relevant to the conditions of sample extraction for brute-force hyperpolarization. As in recent work,[5,7] preparation for sample ejection requires bringing the sample-handling system to positive pressure with concurrent warming to about 10–12 K. In spite of a pre-cooled sample path, some additional warming likely also occurs during ejection itself.

Thus, to extend the relevance of the current work, we compared LFTM at 4.2, 10 and 15 K by collecting full 2D sets *vs.* t_{mix} and B_{mix} from the non-annealed, well-deoxygenated sample. Fig. 5(a–c) plots the I_0, τ and T_{1m}, respectively, as obtained from fitting each constant-B_{mix} slice at each temperature to eqn (1). Comparing 4.2 and 10 K, little-to-no differences were observed in the profiles of these parameters *vs.* B_{mix}. This is consistent with our separate observation of essentially identical mixing at 50 G in the intermediate-annealed sample at 4.2 and 10 K

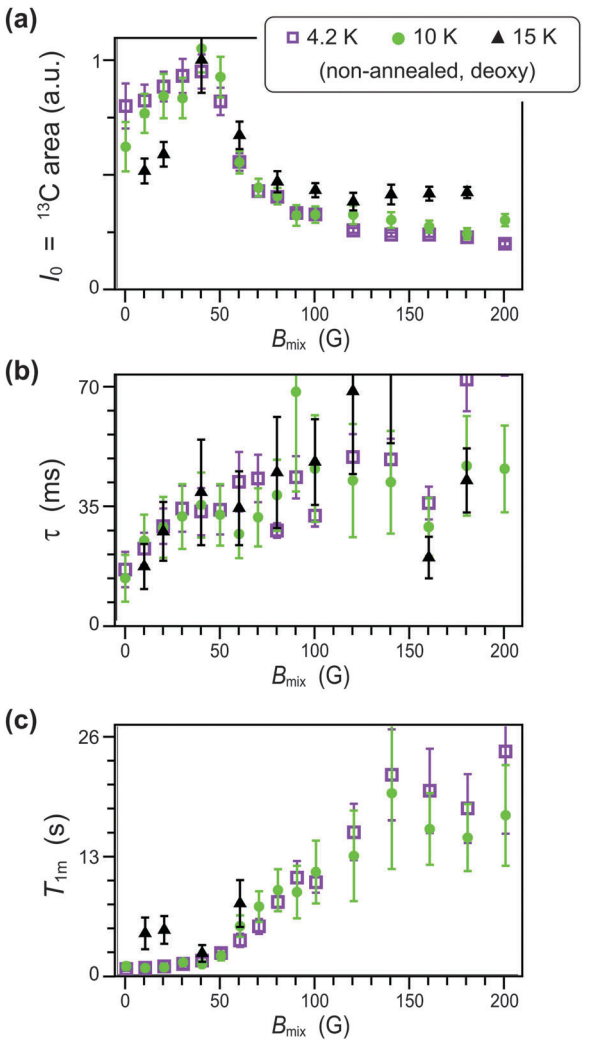

Fig. 5 Impact of temperature on mixing parameters *vs.* B_{mix}, including data at 4.2 K (□), 10 K (●) and 15 K (▲). Showing (a) I_0, the ^{13}C intensity, (b) τ, the ^{1}H–^{13}C mixing time constant, and (c) T_{1m}, the common relaxation time constant for decay of order in the ^{1}H–^{13}C spin system. The 4–20 K range is thought to be most relevant for mixing as utilized in recent brute-force hyperpolarization experiments.[5,7] In (c), T_{1m} values at 15 K include only fitted results whose uncertainty was $<100\%$. Large uncertainties there are due to a combination of poor-signal-to-noise and a maximum value of t_{mix} that was insufficient for full decay.

This journal is © the Owner Societies 2016

Open Access Article. Published on 24 June 2016. Downloaded on 8/12/2024 11:40:28 PM.
This article is licensed under a Creative Commons Attribution 3.0 Unported Licence.

(see Materials and Methods). Characterizations at higher temperatures were challenging due to poor signal-to-noise. Without resorting to long signal averaging, the 15 K set was near the threshold of detection and attempts at 20 K were not quantifiable. Nonetheless, 15 K results in Fig. 5 show the same general patterns as at the lower temperatures. In particular, no significant changes in τ are apparent and the few T_{1m} points available (limited by data quality) do not suggest increased rates of polarization loss.

Discussion

A key overall finding here is that beneficial ^{13}C polarization build-up from ^{1}H–^{13}C equilibration (at $1/\tau$) is much faster than the detrimental approach (at $1/T_{1m}$) to the near-zero thermal-equilibrium polarizations of low mixing fields (*e.g.*, <500 G). We observed $(1/\tau) \sim 10^3 \times (1/T_{1m})$ all tested conditions ($T = 4$–15 K and $B_{mix} = 0$–200 G). This is consistent with earlier analysis[5] of the very low losses observed in seminal brute-force experiments, where it was argued that no more than 5% loss could be due to thermal mixing. Low losses ($\sim$10–30%) were also observed by Gadian *et al.*[4] using LFTM to equilibrate ^{1}H polarization with either ^{13}C or ^{31}P in field-swept brute-force studies without sample ejection. In spite of those successes, high-efficiency LFTM should not be taken for granted, as evidenced by the poor equilibration of hyperpolarized ^{129}Xe with co-solidified ^{13}C-labeled molecules (variously reported at 0.1–5% efficient[33–35]). Those difficulties might be partly attributed to distinct spin physics with ^{129}Xe, but were most likely due to poor dipolar contact in inhomogeneous mixtures. That problem was uniquely imposed by the method of condensing dissimilar components (xenon and target molecule) and is of no concern in our exploration of neat molecules, nor is it likely to be important on extension to frozen solutions.

It is, however, valuable to consider what guidance the present results provide for LFTM in other samples. For example, brute force hyperpolarization has been demonstrated in other molecules, although enhancements were smaller and the role of LFTM was not clear.[5] First, one lesson here can readily be taken as general: avoid opportunities for O_2 or other paramagnetic impurities to infiltrate the sample. The resulting electron-induced relaxation should be similarly detrimental across a variety of samples. Barring that, consider how the quality of unadulterated mixing may vary *vs.* sample type. The first key factors are the dipolar linewidths of interacting nuclei. The LFTM equilibration time τ is a function of the spectral overlap of the interacting spins, which is set by the linewidths and the degree of separation between lines.[1–3] The widths are independent of field, whereas separation is given by $B_{mix}(\gamma_h - \gamma_l)$, where γ_h and γ_l are for high- and low-γ nuclei. Of course, linewidths vary somewhat among molecules. Indeed, [1-^{13}C] pyruvic acid exhibits different values *vs.* its morphology, *e.g.*, ^{1}H ranging from 25 to 35 kHz from non- to fully annealed. For molecular targets with a distinct low-γ nucleus, the magnitude of dipolar interactions and degree of spectral separation *vs.* B_{mix} will also differ. That can alter τ and shift optimum position for LFTM *vs.* (B_{mix}, t_{mix}).

In spite of differing linewidths, effects on τ are slight, as seen for non- *vs.* intermediate-annealed forms in the present study [Fig. 4(b)]. For distinct molecules, linewidth variations will typically be of similar scale as with pyruvic acid morphologies, thus similarly small changes in τ ($\sim$20%) are anticipated. Beyond neat samples, the same general timescale is reasonably expected for solvated molecules, assuming a solvent with similar proton density. That is consistent with the findings of Gadian *et al.*,[4] which demonstrated effective LFTM for sodium [1-^{13}C] acetate, both in water–glycerol solution and in powder form, on timescales ($\sim$100 ms) similar to τ values observed here. In solution, the low-γ spin on the target molecule will equilibrate according to dominant solvent ^{1}H polarization and the dipolar interactions of those protons with the target nucleus. Even in challenging cases of particularly narrow lineshapes, resulting slower equilibration would be tolerable. For example, a rough requirement is that build-up be about 10$\times$ faster than decay, and the factor of $\sim 10^3$ observed in the work presented here leaves significant flexibility.

Variations in T_{1m} from molecule to molecule and for solvated *vs.* neat molecules may be more important for future considerations. Unlike τ, which depends on coherent dipolar evolution (similar to spin diffusion), T_{1m} reflects relaxation governed by incoherent fluctuations of the dipolar interaction. The cause is molecular motion. Of course, that can vary significantly among sample types. Importantly, we have also shown here that in [1-^{13}C] pyruvic acid T_{1m} sits just above a comfort threshold. That is, for at least the non-annealed form, T_{1m} is only a bit longer than the $\sim$1 s required to eject a sample from a brute-force polarizer (400–500 ms of that in an LFTM active field). Thus it will be valuable in future work to characterize and understand variations in T_{1m} among a variety of targets for brute-force hyperpolarization. One may also consider simply applying a field to part of the ejection path in order to reduce transit time through LFTM-active conditions.

Conclusions

We detailed ^{1}H–^{13}C thermal mixing in neat [1-^{13}C] pyruvic acid at the cryogenic temperatures ($\leq$15 K) operative during sample extraction from a brute-force hyperpolarization apparatus.[5,7] There, LFTM is used to take advantage of $\sim$10$\times$ faster ^{1}H build-up times compared to the target of hyperpolarization, ^{13}C. Such low-γ nuclei are excellent candidates as imaging agents due to long solution-state polarization lifetimes, the opportunities for background-free detection and tracing metabolic conversion or other signatures of tissue health.

Results here map out parameters for effective LFTM with unprecedented detail. This reveals an excellent match with fields and exposure times employed for sample ejection in noted brute-force studies. Importantly, we also quantified the beneficial impacts of annealing and deoxygenation for LFTM. Excluding O_2 was clearly valuable in order to limit decay during mixing, doubling of the lifetime (T_{1m}) of spin order during active LFTM. At the same time, the intermediate-annealed state

Open Access Article. Published on 24 June 2016. Downloaded on 8/12/2024 11:40:28 PM.
This article is licensed under a Creative Commons Attribution 3.0 Unported Licence.

of frozen pyruvic acid exhibited a further doubling of T_{1m}. Rapid growth of ^{13}C polarization during mixing, combined with much slower decay of ^{1}H–^{13}C order (*i.e.*, $T_{1m} \gg \tau$), suggests that LFTM can be exploited with almost no loss.

It was also essential to determine the low-field threshold for active mixing. That is because, some circumstances require turning off mixing in order to prevent destruction of polarization on the low-γ nucleus *via* contact with unpolarised protons. For example, long ^{13}C lifetimes can enable transport of ^{13}C hyperpolarization from the polarizer to an imaging centre, although faster relaxing ^{1}H polarization typically disappears during transport. In the recent demonstration of such transport with hyperpolarized [1-^{13}C] pyruvic acid,[7] the sample was transported in modest high field and then passed in to a dissolution apparatus before imaging. In that final passage a 300 G 'magnetic tunnel' was used to prevent destructive LFTM. Here we have shown that this was more than sufficient and also set guidelines for future work.

Finally, it is worthwhile to comment on roles for LFTM beyond brute-force. LFTM is operative in solids only, yet it cannot be generally utilized with other solids-to-liquids hyperpolarization methods, such as d-DNP. That is because the vast majority of current d-DNP experiments require intimate contact of electron spins with the nuclear bath.¶ For LFTM conditions, the electrons would cause rapid relaxation to zero of all nuclear polarization,[37,38] much as we observed with O_2. Thus, d-DNP utilizes dissolution at high field within the polarizing cryostat, extracting the sample *via* the dissolution process itself. Brute force has been unique for its ability to extract a hyperpolarized solid, and thereby utilize LFTM and also enable remote transport. We also note one last advantage of LFTM *vs.* more-familiar NMR techniques to transfer polarization from ^{1}H to low-γ spins (*e.g.*, spin-locked cross polarization[39]). LFTM avoids both RF heating and confinement of the sample to an RF coil, and thus maintains the scalability of brute force to larger samples and/or to multi-sample production. This is a key advantage of brute force, especially important in comparison to higher throughput hyperpolarization methods like d-DNP.

Experimental

Samples

Neat 1-^{13}C (99%) pyruvic acid was purchased from Cambridge Isotope Labs (Tewksbury, MA, USA). Purchased quantities were deoxygenated by 5–10 freeze–pump–thaw cycles and kept in the −30 °C freezer of our N_2-atmosphere drybox. All samples originated from this deoxygenated stock, including the O_2-exposed case.

Sample sealing and O_2 exposure

Space available in the FFC apparatus required a very short (<20 mm) sample tube, and alternative sealing approach *vs.* the flame-sealing approach noted in separate publications.[7] Here, short sample tubes were 5 mm OD (4 mm ID) Suprasil (synthetic quartz) purchased from Wilmad (Vineland, NJ, USA). These included a custom 5 mm-long constriction to about half of the ID and centered 18 mm from the bottom of the tube. Tubes were broken off by scoring and snapping at the constriction, and then the surface was roughed by gentle external filing at the neck and top surface, as shown in Fig. 6(a). Tubes were then soaked several minutes in 0.25 M ethylenediaminetetraacetic acid (EDTA), thoroughly rinsed with ultralow-metal-content Chromosolv LC-MS water and vacuum dried. The EDTA and water were from Sigma Aldrich (St. Louis, MO, USA).

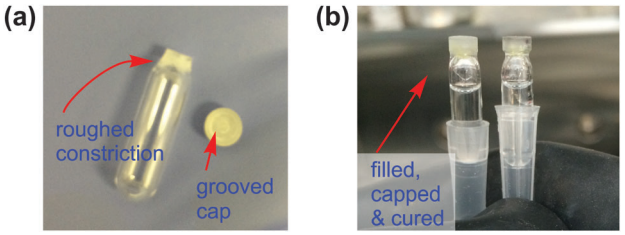

Fig. 6 Sample tubes for cryo-tolerant sealing and exclusion of O_2. (a) Empty tube and cap as prepared for sample loading. Opaque quality of the cap is due to addition of finely ground quartz. (b) Two tubes, as filled with neat [1-^{13}C] pyruvic acid, capped and cured in the dry box.

A cap for airtight, cryo-tolerant sealing was formed as follows. An approximately 3 : 1 mix of Stycast 1266 epoxy (Ellsworth Adhesives, Germantown, WI, USA) and finely ground quartz was cured in a cylindrical Teflon form with 5 mm diameter. A 0.5 mm wide circular groove was machined out of the hardened cylinder so the cap [Fig. 6(a)] mates inside and out with the constricted sample tube. A similar clean-and-rinse protocol was applied to the cap as for sample tubes. In the drybox, ~160 μL of deoxygenated [1-^{13}C] pyruvic acid was carefully pipetted to each sample tube. Stycast 1266 resin and hardener were freshly mixed in the drybox, and a thin layer was spread outside the tube constriction, on the top surface, and on the cap. These were press fit, held upright while curing in the drybox for >24 hours at room temperature. The final product is shown in Fig. 6(b).

The 'O_2-exposed' sample was not sealed in this manner. It was likewise prepared in the drybox using deoxygenated [1-^{13}C] pyruvic acid. However, it was then sealed using only tightly packed, degassed Teflon tape at the end of a cut (~20 mm long) and cleaned Suprasil NMR tube filled with 200–300 μL of sample. Finally, tight external taping with Teflon (or parafilm to similar result) was used. Evidently, and in spite of only brief (≤5–10 min) exposure to air at room-temperature, such 'seals' were too permeable to maintain deoxygenation. Several samples prepared in this way yielded T_1 profiles as shown for the 'O_2-exposed' sample in Fig. 1(a). Nonetheless, these poorly sealed cases proved serendipitous in that corresponding data enabled us to explore the effects of O_2 contamination on both T_1 *vs.* temperature and LFTM.

Finally, we note that present, relatively large samples must be less sensitive to O_2 exposure than the high surface-to-volume

¶ As promising alternative, Jannin and coworkers demonstrated 'remote' DNP,[36] which starts with DNP to solvent ^{1}H spins in contact with solute free radicals. That traditional step is followed by spin diffusion to protons in molecules forming dispersed crystallites that are isolated from the free radicals. Finally, cross polarization yields hyperpolarized ^{13}C in the isolated targets. The physical separation can allow controlled two-spin LFTM (*e.g.*, of ^{1}H and ^{13}C), as well as production of transportable hyperpolarization.

This journal is © the Owner Societies 2016

Open Access Article. Published on 24 June 2016. Downloaded on 8/12/2024 11:40:28 PM. This article is licensed under a Creative Commons Attribution 3.0 Unported Licence.

ratio samples used in prior brute-force work.[5] Thus, the demonstrated detrimental effects of O_2-exposure urge particular caution for such preparations of a sample.

Sample annealing

The procedure was similar to that presented elsewhere,[7,32] here implemented directly in the FFC apparatus. It was applied to the sample already characterized as non-annealed (and well-deoxygenated) without melting or removing it from the helium-flow cryostat and NMR probe. The initial non-annealed state was generated by freezing the liquid sample (m.p. = 285 K) from room temperature to <200 K in $\sim$20–30 min. Non-annealed, intermediate- and fully annealed forms are stable below $\sim$215 K for at least as long as yet monitored (>4 days). After $\sim$2 days characterization of the non-annealed form, measuring $T_1(^1H)$ between 4–120 K, and LFTM over 4–20 K, we then proceeded to generate the intermediate-annealed form. For this, the sample was left overnight ($\sim$8 h) at $\sim$243 K and then dropped quickly ($\sim$20 m) to 200 K. After this, T_1 values were obtained at 200, 80 and 10 K before proceeding to characterization of LFTM. The 243 K annealing temperature was chosen to correspond with the freezer temperature where samples were held in preparation for earlier brute-force hyperpolarization experiments.[5]

Fast field cycling (FFC) and cryogenic systems

Experiments were performed on the FFC apparatus at the University of Nottingham, as described previously by Horsewill and Xue.[40] Low-inductance (20 mH) superconducting magnet at 4.2 K and fast-ramping power supply from Cryogenic, Ltd (London, UK) provide fields between 0 to 2.5 T with ramping rate up to 10 T s^{-1}. The system includes an integrated helium flow cryostat that sips helium from the magnet reservoir. Temperature is maintained *via* a Lakeshore 331 controller coupled to resistive heater in the helium flow path. Sample temperature is reported by a calibrated Cernox sensor in good thermal contact with a brass block surrounding the NMR sample and coil. Temperature stability was $\leq(\pm 0.05$ K) for runs approaching 24 h. Min, max and mean values were recorded with each fixed-B_{mix} profile of intensity *vs.* t_{mix}, and with each recovery trace to measure T_1.

Field stability and reproducibility in this apparatus have been estimated to be about $\pm$1.5 G based on the standard deviation of repeated ^{1}H NMR measurements, each collected following a field-cycling event.[40] Rechecking here, we similarly estimated reproducibility of $\pm$5 G *via* the RMS deviations of fitted peak positions from in ^{13}C spectra represented in the 2D arrays of Fig. 3(a–c). Only spectra above signal-to-noise of 60 were used, or about $\sim$75 spectra from each array. (Note, the observed range was $\pm$20 G.) Each spectrum involved cycling events and settling time (40 ms) described in Fig. 2. Finally, we believe any offset field (*e.g.*, due to flux trapping by the superconducting magnet of the $\sim$0.25–0.65 G earth field), was likely smaller than the noted variation in field stability. This is based in the indistinguishability of the 2D data set (*vs.* B_{mix} and t_{mix}) in Fig. 3(a) from another collected immediately after on the same sample, but with reversed polarity of the magnet.

NMR apparatus

The NMR probe contains a single solenoid coil tuned to about 21.6 MHz. Different nuclei were addressed by adjusting the field to $B_0 = \gamma_n^{-1} \times$ (21.6 MHz), where γ_n is the gyromagnetic ratio. The NMR spectrometer was operated by home-written code in visual basic. Automated data-collection steps through values of B_{mix}, t_{mix} and temperature were similarly controlled by home-written software.

Data processing and analysis

Processing and analysis was performed using *Mathematica*. Time-domain signals were multiplied by a matched exponential window (20 and 5 kHz for ^{1}H and ^{13}C), Fourier transformed and autophased. ^{13}C intensities were obtained by integrating the frequency domain over $\pm$50 kHz about the center frequency, and similarly for ^{1}H spectra in T_1 experiments.

Parameters of thermal mixing were determined by fitting to eqn (1) using *Mathematica*'s standard routine for nonlinear regression. Error bars in Fig. 4 and 5 are the asymptotic standard errors reported by the fitting routine These may underestimate uncertainty in cases where data trends do not strictly follow eqn (1), as discussed in the main text.

NMR experiment parameters

Thermal-mixing experiments using the pulse sequence of Fig. 2 had $t_{polarize}$ = 40 s at 4.2 K in the case of non-annealed, O_2-exposed samples. Due to the longer T_1 of the non-annealed, well-deoxygenated sample at 4.2 K (see Fig. 1), we used correspondingly longer polarization time of 150 s. Meanwhile, experiments on that sample at 10, 15 and 20 K used $t_{polarize}$ = 100, 40 and 20 s, respectively. For the intermediate-annealed (and well-deoxygenated) sample, we used $t_{polarize}$ = 200 s at 4.2 K and 150 s at 10 K.

The NMR excitation and detection frequency was 21.6 MHz, corresponding to B_0 = 2.018 T for ^{13}C or 0.507 T for ^{1}H. T_1 experiments in the FFC apparatus were by saturation recovery, the same as performed in earlier experiments[7] with a static-field system at 2 and 4 T. Here, ^{1}H saturation recovery occurred at 2.0 T, followed by detection at the resonant field (0.507 T). That was achieved using a field-cycling pulse sequence similar to that in Fig. 2. Pulse times for ^{1}H and ^{13}C were typically t_{90} = 2 and 8 μs. Single-scan ^{13}C spectra were collected in 512 complex time-domain points at 0.3 s dwell time (3.3 MHz spectral width). Similar parameters were used for ^{1}H-detected experiments to measure $T_1(^1H)$.

The time required to collect a full 2D series of thermal-mixing results depended on the polarization time and the size of the set of t_{mix} and B_{mix} values used. The longest running 2D series [Fig. 3(c), $t_{polarize}$ = 150 s] required $\sim$17 h for 18 values of t_{mix} from 1 ms to 12 s in regular increments of 0.24 log units and 19 values of B_{mix} ranging 0 to 100 G in increments of 10 G, then 120 to 200 G in increments of 20 G, and finally 250, 300 and 350 G. Plots in Fig. 3(a–c) also incorporate slices at B_{mix} = 110, 130, 150, 170, 190 G that were linearly interpolated from nearest neighbors in order to plot regular 10 G intervals

Open Access Article. Published on 24 June 2016. Downloaded on 8/12/2024 11:40:28 PM.
This article is licensed under a Creative Commons Attribution 3.0 Unported Licence.

over 0–200 G. Data sets above 200 G revealed very little ^{13}C intensity, and are not shown in either Fig. 3(a–c) or in the plots of fitted parameters *vs.* B_{mix} in Fig. 4 and 5.

Finally, due to longer polarization times for the intermediate-annealed sample, collection of a full 2D set at 4.2 K was less practical than at 10 K. Nonetheless, as noted in the caption to Fig. 3, this sample exhibited nearly indistinguishable LFTM behavior at these two temperatures for the 50 G 'mixing optimum'. Specifically, τ = (40.0 ± 8.4) ms and T_{1m} = (6.1 ± 1.2) s at 4.2 K, *vs.* (38.5 ± 8.5) ms and (5.0 ± 1.1) s at 10 K.

Acknowledgements

We thank Andy Stewart from the Univ. of Nottingham Physics and Astronomy electronics shop for occasional repairs of the NMR probe. We thank Werner Maas of Bruker Biospin for encouragement and support of the project.

Notes and references

1 A. Abragam and W. G. Proctor, *Phys. Rev.*, 1957, **106**, 160–161.
2 A. Abragam and W. G. Proctor, *Phys. Rev.*, 1958, **109**, 1441–1458.
3 A. Abragam, *Principles of Nuclear Magnetism*, Clarendon Press, Oxford, 1961.
4 D. G. Gadian, K. S. Panesar, A. J. P. Linde, A. J. Horsewill, W. Kockenberger and J. R. Owers-Bradley, *Phys. Chem. Chem. Phys.*, 2012, **14**, 5397–5402.
5 M. A. Hirsch, N. Kalechofsky, A. Belzer, M. M. Rosay and J. G. Kempf, *J. Am. Chem. Soc.*, 2015, **137**, 8428–8434.
6 J. R. Owers-Bradley, A. J. Horsewill, D. T. Peat, K. S. K. Goh and D. G. Gadian, *Phys. Chem. Chem. Phys.*, 2013, **15**, 10413–10417.
7 M. L. Hirsch, B. A. Smith, M. Mattingly, A. G. Goloshevsky, M. Rosay and J. G. Kempf, *J. Magn. Reson.*, 2015, **261**, 87–94.
8 J. H. Ardenkjær-Larsen, B. Fridlund, A. Gram, G. Hansson, L. Hansson, M. H. Lerche, R. Servin, M. Thaning and K. Golman, *Proc. Natl. Acad. Sci. U. S. A.*, 2003, **100**, 10158–10163.
9 C. R. Bowers and D. P. Weitekamp, *J. Am. Chem. Soc.*, 1987, **109**, 5541–5542.
10 R. W. Adams, J. A. Aguilar, K. D. Atkinson, M. J. Cowley, P. I. P. Elliott, S. B. Duckett, G. G. R. Green, I. G. Khazal, J. López-Serrano and D. C. Williamson, *Science*, 2009, **323**, 1708–1711.
11 F. Reineri, T. Boi and S. Aime, *Nat. Commun.*, 2015, **6**, 5858.
12 P. Höfer, G. Parigi, C. Luchinat, P. Carl, G. Guthausen, M. Reese, T. Carlomagno, C. Griesinger and M. Bennati, *J. Am. Chem. Soc.*, 2008, **130**, 3254–3255.
13 K. G. Valentine, G. Mathies, S. Bédard, N. V. Nucci, I. Dodevski, M. A. Stetz, T. V. Can, R. G. Griffin and A. J. Wand, *J. Am. Chem. Soc.*, 2014, **136**, 2800–2807.
14 L. T. Kuhn, *Top. Curr. Chem.*, 2013, **338**, 229–300.
15 B. M. Goodson, Y. Song, R. E. Taylor, V. D. Schepkin, K. M. Brennan, G. C. Chingas, T. F. Budinger, G. Navon and A. Pines, *Proc. Natl. Acad. Sci. U. S. A.*, 1997, **94**, 14725–14729.
16 M. M. Spence, S. M. Rubin, I. E. Dimitrov, E. J. Ruiz, D. E. Wemmer, A. Pines, S. Q. Yao, F. Tian and P. G. Schultz, *Proc. Natl. Acad. Sci. U. S. A.*, 2001, **98**, 10654–10657.
17 C. Boutin, H. Desvaux, M. Carrière, F. Leteurtre, N. Jamin, Y. Boulard and P. Berthault, *NMR Biomed.*, 2011, **24**, 1264–1269.
18 Y. Bai, P. A. Hill and I. J. Dmochowski, *Anal. Chem.*, 2012, **84**, 9935–9941.
19 N. S. Khan, B. A. Riggle, G. K. Seward, Y. Bai and I. J. Dmochowski, *Bioconjugate Chem.*, 2015, **26**, 101–109.
20 R. Sriram, J. Kurhanewicz and D. B. Vigneron, *eMagRes*, 2014, **3**, 311–324.
21 S. Meier, P. R. Jensen, M. Karlsson and M. H. Lerche, *Sensors*, 2014, **14**, 1576–1597.
22 K. M. Brindle, *J. Am. Chem. Soc.*, 2015, **137**, 6418–6427.
23 S. J. Nelson, J. Kurhanewicz, D. B. Vigneron, P. E. Larson, A. L. Harzstark, M. Ferrone, M. van Criekinge, J. W. Chang, R. Bok, I. Park, G. Reed, L. Carvajal, E. J. Small, P. Munster, V. K. Weinberg, J. H. Ardenkjaer-Larsen, A. P. Chen, R. E. Hurd, L. I. Odegardstuen, F. J. Robb, J. Tropp and J. A. Murray, *Sci. Transl. Med.*, 2013, **5**, 198ra108.
24 S. E. Day, M. I. Kettunen, F. A. Gallagher, D.-E. Hu, M. Lerche, J. Wolber, K. Golman, J. H. Ardenkjaer-Larsen and K. M. Brindle, *Nat. Med.*, 2007, **13**, 1382–1387.
25 T. Harris, G. Eliyahu, L. Frydman and H. Degani, *Proc. Natl. Acad. Sci. U. S. A.*, 2009, **106**, 18131–18136.
26 K. M. Brindle, S. E. Bohndiek, F. A. Gallagher and M. I. Kettunen, *Magn. Reson. Med.*, 2011, **66**, 505–519.
27 D. M. Wilson and J. Kurhanewicz, *J. Nucl. Med.*, 2014, **55**, 1567–1572.
28 Y. Li, I. Park and S. J. Nelson, *Cancer J.*, 2015, **21**, 123–128.
29 O. J. Rider and D. J. Tyler, *J. Cardiovasc. Magn. Reson.*, 2013, **15**, 1–9.
30 C. Purmal, B. Kucejova, A. D. Sherry, S. C. Burgess, C. R. Malloy and M. E. Merritt, *Am. J. Physiol.*, 2014, **307**, H1134–H1141.
31 A. J. Bakermans, D. Abdurrachim, R. P. M. Moonen, A. G. Motaal, J. J. Prompers, G. J. Strijkers, K. Vandoorne and K. Nicolay, *Prog. Nucl. Magn. Reson. Spectrosc.*, 2015, **88–89**, 1–47.
32 J. G. Kempf, N. Kalechofsky and M. Rosay, *US Pat.*, US2015061666 (A1), 2014.
33 C. R. Bowers, H. W. Long, T. Pietrass, H. C. Gaede and A. Pines, *Chem. Phys. Lett.*, 1993, **205**, 168–170.
34 A. Cherubini, G. S. Payne, M. O. Leach and A. Bifone, *Chem. Phys. Lett.*, 2003, **371**, 640–644.
35 N. Lisitza, I. Muradian, E. Frederick, S. Patz, H. Hatabu and E. Y. Chekmenev, *J. Chem. Phys.*, 2009, **131**, 044508.
36 A. Bornet, X. Ji, B. Vuichoud, J. Milani, D. Gajan, A. J. Rossini, L. Emsley, G. Bodenhausen and S. Jannin, Joint 5th International DNP Symposium and COST Action EuroHyperpol, Egmond aan Zee, The Netherlands, 2015.
37 D. T. Peat, A. J. Horsewill, W. Kockenberger, A. J. P. Linde, D. G. Gadian and J. R. Owers-Bradley, *Phys. Chem. Chem. Phys.*, 2013, **15**, 7586–7591.
38 S. Macholl, H. Johannesson and J. H. Ardenkjaer-Larsen, *Phys. Chem. Chem. Phys.*, 2010, **12**, 5804–5817.
39 A. Pines, M. G. Gibby and J. S. Waugh, *J. Chem. Phys.*, 1972, **56**, 1776–1777.
40 A. J. Horsewill and Q. Xue, *Phys. Chem. Chem. Phys.*, 2002, **4**, 5475–5480.